Measurement 213 (2023) 112728

Contents lists available at ScienceDirect

Measurement

journal homepage: www.elsevier.com/locate/measurement

Two proposals to simplify resistive sensor readout based on Resistance-to-Time-to-Digital conversion

José A. Hidalgo-López [a,*], Julián Castellanos-Ramos [a,b]

[a] Departamento de Electrónica, Universidad de Málaga, Andalucía Tech, Campus de Teatinos, Málaga 29071, Spain
[b] Instituto de Investigación Biomédica de Málaga (IBIMA), Málaga 29010, Spain

ARTICLE INFO

Keywords:
Direct interface circuits
Resistance-to-time-to-digital conversion
Resistive sensor
Time-based measurement

ABSTRACT

Direct Interface Circuits (DICs) are simple circuits used in readouts for all types of sensors. For resistive sensors, all DICs perform a resistance-to-time-to-digital conversion using just the sensor, some calibration resistors, one or two capacitors, and a Digital Processor. These circuits require a variable number of charging and discharging cycles of a capacitor to estimate the sensor resistance, R_x, increasing both acquisition time and power consumption. This paper presents two resistive DICs capable of estimating R_x by means of a single charging-discharging process, simplifying the readout process. Furthermore, this is achieved without increasing hardware requirements. Only two time measurements are used to obtain R_x. Despite the simplicity of the new circuits, the experimental results show that relative errors of estimating R_x can be below 0.8 %, and this in a wide range of resistances of over 40 dB. Moreover, acquisition time and energy consumption can be reduced by up to 75 %.

1. Introduction

Resistive sensors interfaced with digital systems play a crucial role in data acquisition for numerous applications. These applications come in all types, such as resistance temperature detectors (RTD) [1], gas sensors [2], and gait analysis [3], among many others. The widespread use of resistive sensors increases the importance of designing efficient circuits to obtain digital resistance measurements. From an electronic design point of view, different approaches can be used for the readout, such as the one based on so-called Direct Interface Circuits (DICs). These circuits stand out for their simplicity since they only need some passive elements and a Digital Processor (DP) in their most basic versions. This DP is solely to control the processes required for readout, to measure time intervals (for which a timer is needed), and it can also perform the arithmetic operations that provide the final result.

In a large number of applications, the DPs are microcontrollers [4–15], although field-programmable gate arrays (FPGAs) [16,17] are also used. In [4,5,8,9,12,13,16,17] single resistive sensor readout circuits with only passive components are implemented. In [7], a DC voltage source is added to the circuit for the same purpose. Other versions of resistive DICs can include transistors and triggers [11], or operational amplifiers (OAs) and switches as external elements to the DP [6,10,14,15], but always keeping the number of components to a minimum. None of these circuits need to incorporate analog-to-digital converters (ADCs). The DIC actually performs a time-to-digital-to-resistance conversion in which the time measurements come from carrying out several capacitor charging-discharging processes. These measurements are performed by the DP itself and will therefore be expressed in a number of cycles of its internal clock. Finally, it is important to note that DICs can also be used for the readout of inductive and capacitive sensors [18–21].

Among the resistive DICs that use only passive components, the Two-Point Calibration Method [22,23] (TPCM) stands out for the excellent trade-off between the number of components required, the simplicity of the readout processes, and the accuracy of the results. The circuit used in the TPCM is shown in Fig. 1 (a). In addition to the DP and the sensor, R_x, two calibration resistors of known values, R_{c1} and R_{c2}, are required, along with a capacitor, C. Some implementations of this DIC include a resistor between the Pp pin and C with a dual purpose: to reduce charging current if necessary and to reduce noise at Vo [23]. The operation principle is simple: three charging cycles of C are performed, and the capacitor is discharged through one of the resistors after each one. It must be possible to configure the DP pins as inputs (high-impedance state, Hi-Z) or outputs in order to carry out these processes. During discharge, the pin connected to the capacitor in Fig. 1 (a) is configured as input (Hi-Z state) to detect the trigger instant during

* Corresponding author.
E-mail addresses: jahidalgo@uma.es (J.A. Hidalgo-López), jcramos@uma.es (J. Castellanos-Ramos).

https://doi.org/10.1016/j.measurement.2023.112728
Received 25 March 2022; Received in revised form 14 February 2023; Accepted 11 March 2023
Available online 20 March 2023
0263-2241/© 2023 The Author(s). Published by Elsevier Ltd. This is an open access article under the CC BY license (http://creativecommons.org/licenses/by/4.0/).

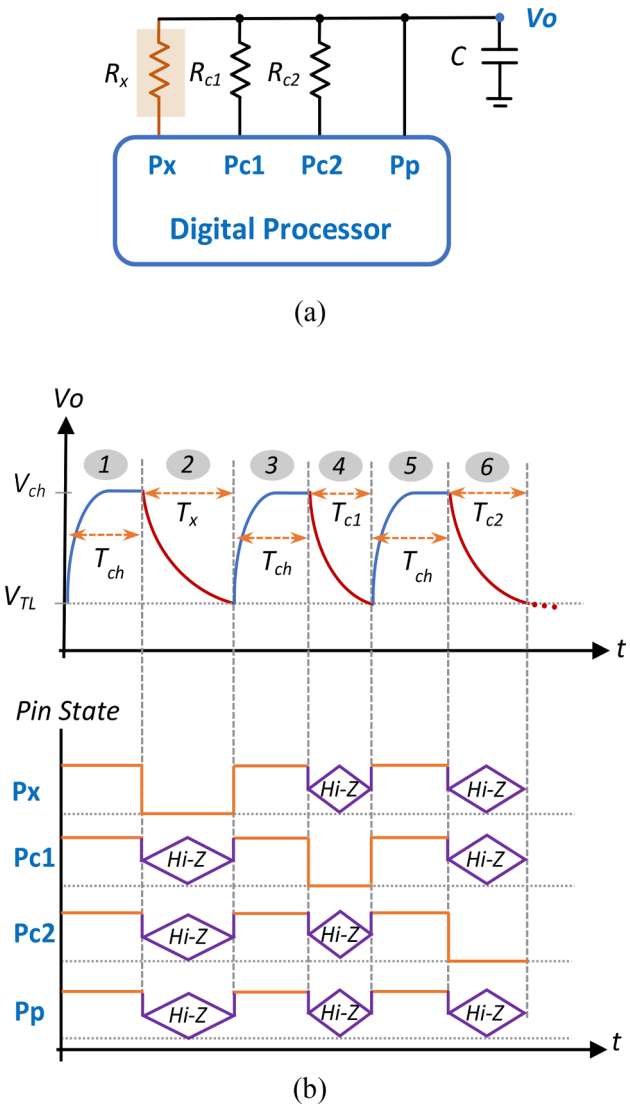

Fig. 1. (a) Classical Two-Point Calibration Method (TPCM) Direct Interface Circuit for the readout of resistive sensor R_x. (b) Steps needed to perform the sensor reading and pin states at each of them.

discharge when the voltage in the capacitor, *Vo*, reaches value V_{TL} (the DP voltage threshold). The DP interprets *Vo* as a logic 0 in the trigger instant, performing three measurements corresponding to the time intervals in which *Vo* is considered as a logic 1 during the three discharges. Fig. 1 (b) shows the waveform of *Vo* and the states of the pins during the three charging and discharging processes of *C*. Times T_x, T_{c1}, and T_{c2} are obtained by discharging through the resistor which has the same subscript (the pins connected to the other resistors must be in a Hi-Z state when discharging through a resistor). Considering the equation for discharging a capacitor through a resistor, *R*, the times measured during discharge would be given by

$$T = (R + ro)C\ln\left(\frac{V_{ch}}{V_{TL}}\right) \tag{1}$$

where *ro* is the output resistance of each pin configured as a logic 0 output, and V_{ch} is the voltage value stored in *C* when starting discharge.

If the charging times, T_{ch} in Fig. 1 (b), are long enough, V_{ch} will coincide with the maximum output voltage that the DP pins can provide, which in most cases coincides with the device's voltage supply, V_{DD}. Considering (1), R_x can be obtained by the expression:

$$R_x = \frac{T_x - T_{c1}}{T_{c2} - T_{c1}}(R_{c2} - R_{c1}) + R_{c1} \tag{2}$$

In this expression, it is not necessary to know the value of *ro*, V_{ch}, *C*, or V_{TL} in order to estimate R_x. However, it should be noted that, for (2) to be valid, V_{ch} must be equal at the end of the three charging processes, therefore making it necessary to use values of T_{ch} that are not negligible compared to discharging times. Moreover, (2) assumes that *ro* is the same in the pins of the three resistors, when in fact there may be small differences between the values simply because they are connected to different resistors. Although the results provided by (2) are good in terms of accuracy, this accuracy decreases for small values of R_x, this being due to several factors [24], including the quantization of the time measurements in clock cycles. The same occurs for large values of R_x, but in this case due to uncertainty in the time measurement. This uncertainty comes from the fact that the slopes of the discharging curves *Vo (t)* are smaller for higher resistance values, making it more difficult to determine the instant at which $Vo = V_{TL}$ [25]. To reduce these problems, [26] includes a second capacitor in series with *C*, and a new measurement pin at the junction of the two capacitors. Two measurements can therefore be taken during each discharge, resulting in greater accuracy when determining R_x.

In any case, three *C* charging and discharging processes are necessary for both the TPCM and the circuit presented in [26]. Hence, the maximum acquisition time for the measurement, $T_{M,TPCM}$, would be given by

$$T_{M,TPCM} = 3{\cdot}T_{ch} + T_{x,\max} + T_{c1} + T_{c2} \tag{3}$$

where $T_{x,\max}$ is the time measured in the discharge through the highest resistance in the range. This means that the process to estimate R_x can be slow. As there are three charging processes, energy consumption without considering the energy consumption of the DP, E_{TPCM}, is given by

$$E_{TPCM} = \frac{3}{2}CV_{DD}^2 \tag{4}$$

which can be high in certain applications. Obviously, the energy consumed by the DPs would have to be added to the previous result to obtain the total energy consumption. However, this can vary greatly depending on the chosen DP. Furthermore, if a microcontroller is selected all its consumption should add up to (4), while if an FPGA is chosen (performing several processes in parallel), only a small fraction of the consumption should add up to (4). Therefore, we will not consider DP consumption to make a fair comparison between different DICs.

There is another simpler DIC, the Single-Point Calibration Method [12] (SPCM), which uses only one calibration resistor and two charging and discharging processes to determine R_x. However, the SPCM does not take *ro* into account in the estimation, meaning errors can be high, especially for resistance values far from the calibration resistance value. In any case, several charging-discharging processes have the objective of eliminating in the estimate of R_x the dependency with *ro*, V_{ch}, *C*, and V_{TL}.

Intending to improve the performance of the DICs found in the literature, this paper presents two DICs with very simple hardware and a straightforward resistive sensor readout process based on a resistance-to-time-to-digital conversion. In the new DICs, the single discharging process is done solely through the sensor (with all pins in a Hi-Z state), eliminating the dependency on *ro*. On the other hand, a procedure based on the ratio of two passive elements removes the dependence on the initial discharge voltage.

In terms of hardware, the new proposals only use, in addition to the DP, passive components in the same or fewer numbers than the TPCM or the one proposed in [26]. The new DICs only use two DP pins, which is between one and three fewer than in other versions, freeing up resources for other uses. There are no calibration processes, thus reducing $T_{M,TCPM}$ (increasing the maximum sampling frequency) while decreasing energy

consumption. However, it is important to point out that, although there are no calibration processes, it is still necessary to know the values of the passive elements used in the new circuits (as occurs, for example, in the TPCM with R_{c1} and R_{c2}) and this could be a source of errors for the circuit. Moreover, the estimation of R_x does not depend on any differences between the *ro* values of the different pins, which helps ensure higher accuracy. Finally, all this is achieved without the need for reference voltage sources, ADCs, or any other type of analog circuitry.

2. The new resistive DIC proposal

Figs. 2 and 3 show the two new DIC proposals. Given the number of capacitors used, the circuit in Fig. 2 will be referred to as the Two-Capacitor Interface (TCI), and the circuit shown in Fig. 3 as the Single-Capacitor Interface (SCI). Each of the proposals is described in detail below.

2.1. The Two-Capacitor Interface, TCI

As shown in Fig. 2 (a), the circuit is very straightforward, consisting simply of two capacitors, C_A and C_B, plus the sensor, R_x. The circuit uses only two DP pins instead of the four pins used by the TPCM in Fig. 1 (a) or the five used in [26]. Fig. 2 (b) shows the waveforms of voltages V_A and V_B during the single charging-discharging process carried out in the circuit to estimate R_x. Likewise, Fig. 2 (b) also shows the pin states during these processes.

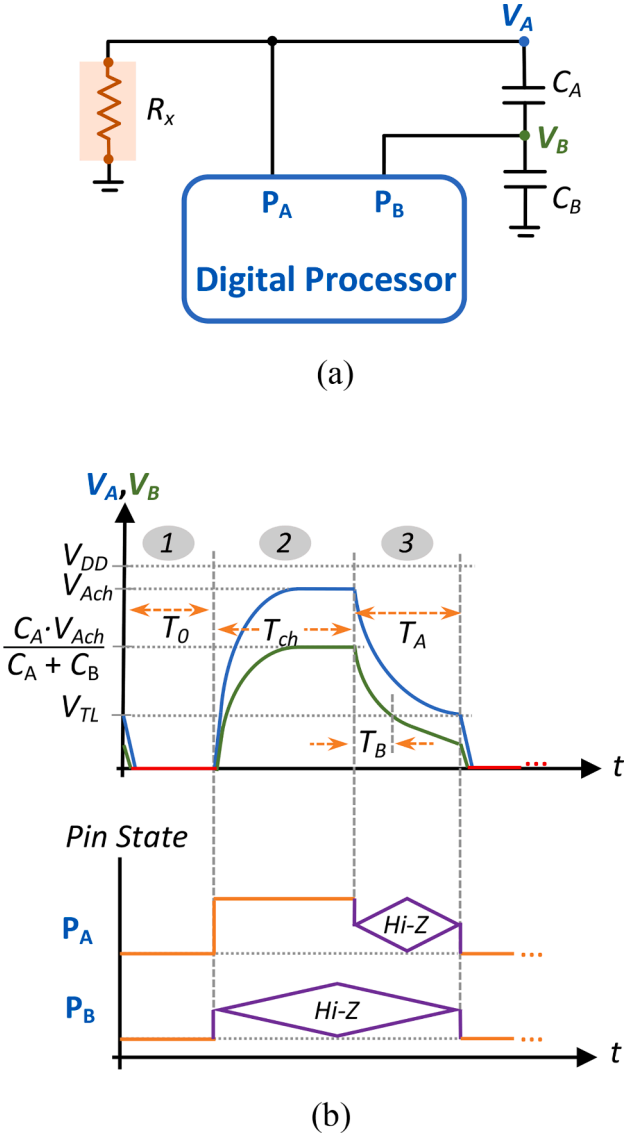

Fig. 2. (a) New Two Capacitor Interface circuit. (b) Waveforms and pin states for the circuit reading process with Fixed charging time, T_{ch} (TCI-F).

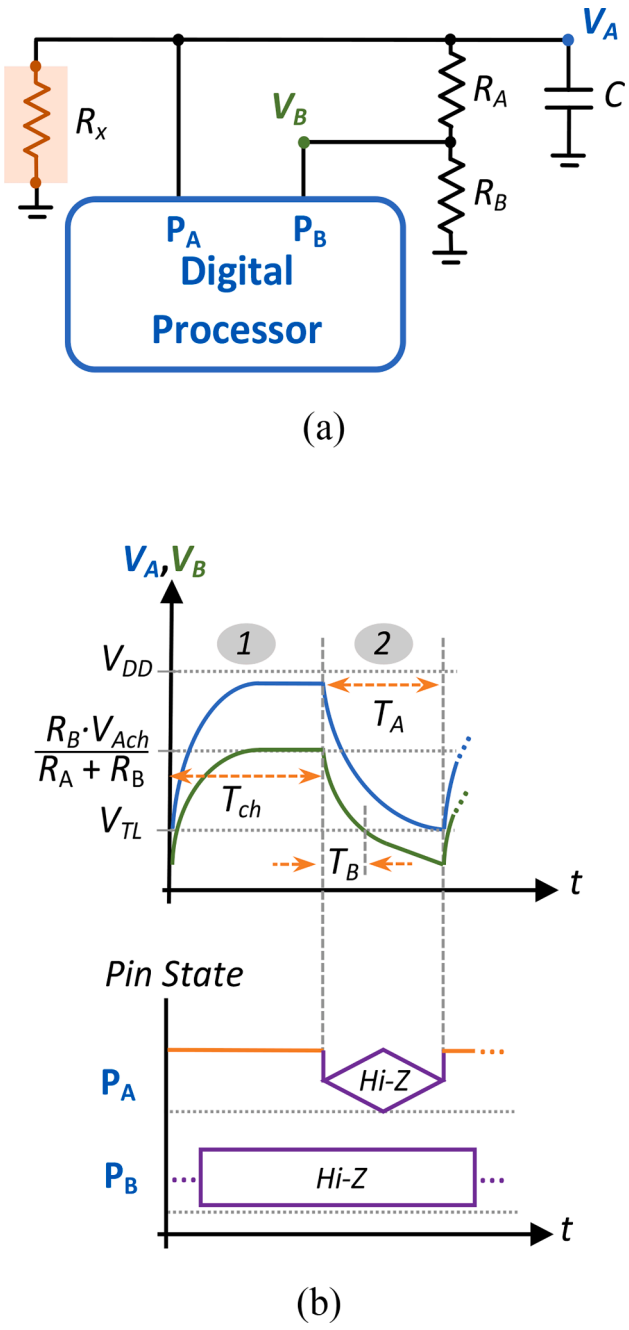

Fig. 3. (a) Proposed Single Capacitor Interface circuit. (b) Waveforms and pin states for the circuit reading process with Fixed charging time, T_{ch} (SCI-F).

The first step in the estimation of R_x (labeled with number 1 in Fig. 2 (b)) is to completely discharge the two capacitors during a fixed time, T_0. To this end, pins P_A and P_B are configured as logic 0 outputs. This step is necessary in order to establish initial voltages equal to 0 in V_A and V_B prior to the charging process that follows.

The next step (the charging process labeled with number 2) is carried out with P_A configured as a logic 1 output while P_B is in Hi-Z state. After a charging time, T_{ch}, V_A stabilizes at $V_A = V_{Ach}$, a value that is close to V_{DD} but lower due to R_x being connected to ground. Moreover, V_{Ach} will

depend on the value of R_x, but as will also be shown, this does not affect the correct operation of the circuit. The final voltage stored in V_B during the charging process, V_{Bch}, is given by:

$$V_{Bch} = \frac{C_A \cdot V_{Ach}}{C_A + C_B} \tag{5}$$

Since the only condition that the TCI circuit must meet to work correctly is $V_{Bch} > V_{TL}$, then the following must be fulfilled:

$$\frac{C_B}{C_A} < \frac{V_{Ach}}{V_{TL}} - 1 \tag{6}$$

This condition ensures that both V_A and V_B are considered as a logic 1 by the DP at the start of discharge. Although it is known that V_{TL} may vary with the operating conditions of the circuit, it will always be possible to find values of C_A and C_B that ensure the difference between the right and left members of (6) are large enough to guarantee the correct operation of the TCI, even if V_{Ach} and V_{TL} are not known precisely.

Charging is followed by discharging, labeled with number 3 in Fig. 2 (b), setting both pins in Hi-Z state. Measurements T_A and T_B, i.e., the time intervals from the start of discharge to the moments when $V_A = V_{TL}$ and $V_B = V_{TL}$ respectively, are obtained in this step. Proceeding as to obtain (1), we find

$$T_A = R_x C_{eq} \ln\left(\frac{V_{Ach}}{V_{TL}}\right) \tag{7}$$

$$T_B = R_x C_{eq} \ln\left(\frac{V_{Bch}}{V_{TL}}\right) = R_x C_{eq} \ln\left(\frac{C_A}{C_A + C_B} \cdot \frac{V_{Ach}}{V_{TL}}\right) \tag{8}$$

where $C_{eq} = C_A \cdot C_B/(C_A + C_B)$. From (7) and (8) it is trivial to find:

$$R_x = \frac{T_A - T_B}{C_{eq} \ln\left(\frac{C_A + C_B}{C_A}\right)} \tag{9}$$

Since C_A and C_B are values chosen by the designer and therefore known, we can store a constant k in the DP:

$$k = \frac{1}{C_{eq} \ln\left(\frac{C_A + C_B}{C_A}\right)} \tag{10}$$

Defining $\triangle T = T_A - T_B$, the final equation for the estimation of R_x is:

$$R_x = k \cdot \Delta T \tag{11}$$

2.2. TCI analysis

Equation (11) has significant advantages over (2). Firstly, only two measurements are necessary to obtain R_x, thus reducing the possible sources of error. Secondly, it is only necessary to store one constant, k, rather than two, R_{c2} - R_{c1} and R_{c1}, as in the TPCM or in [26]. Furthermore, only one subtraction and one multiplication are required in the estimation, rather than two subtractions, one division, one multiplication, and one addition (note that the subtraction done on (11) can be avoided in some DPs if a count can start at time $V_A = V_{TL}$ and end when $V_B = V_{TL}$). Finally, ro does not appear in any of the steps performed to obtain (11), thus avoiding the errors introduced by this element.

Moreover, (11) shows that resolution in the estimation of R_x increases as resolution of $\triangle T$ increases. From (7) and (8), it can be seen that this is achieved by increasing C_{eq} and $(C_A + C_B)/C_A$ (remembering that the designer cannot modify V_{Ach} and V_{TL} once the DP has been chosen). On one hand, C_B/C_A has an upper limit set by (6); and on the other hand, C_{eq} influences T_A and T_B in the same way that C influences the value of T in (1). Although the increase in C_{eq} brings an increase in resolution in R_x, it also causes more uncertainty in the time measurement, $u(T_i)$, as this depends inversely on the slope of the discharging curve when it reaches voltage V_{TL} [27]

$$u(T_i) = \frac{\alpha_i}{\left|\frac{dVo}{dt}\right|_{Vo=V_{TL}}} \approx \frac{\alpha_i R_x C_{eq}}{V_{TL}}; \quad i = A, B \tag{12}$$

where α_i is a parameter related to the noise level in the circuit's node i. From (12), it is easy to find the relative uncertainty in the time measurements

$$\frac{u(T_i)}{\Delta T} \approx \frac{\alpha_i}{V_{TL} \cdot \ln\left(\frac{C_A + C_B}{C_A}\right)} \tag{13}$$

from where relative uncertainty in the estimation of R_x, $u(R_x)/R_x$ is:

$$\frac{u(R_x)}{R_x} = \frac{1}{R_x}\sqrt{\left(\frac{\partial R_x}{\partial T_A}\right)^2 u^2(T_A) + \left(\frac{\partial R_x}{\partial T_B}\right)^2 u^2(T_B)} = \sqrt{\left(\frac{u(T_A)}{\Delta T}\right)^2 + \left(\frac{u(T_B)}{\Delta T}\right)^2} \approx \approx \frac{\sqrt{\alpha_A^2 + \alpha_B^2}}{V_{TL} \cdot \ln\left(\frac{C_A + C_B}{C_A}\right)} \tag{14}$$

This result shows that increasing C_{eq} does not improve the quality of the measurements (once the C_B/C_A ratio is chosen), if T_A and T_B are large enough to disregard the quantization errors. Furthermore, as will be discussed below, any unnecessary increase in C_{eq} brings an increase in the energy dissipated by the TCI.

Energy consumption, E_{TCI}, has three components: the energy dissipated in charging the two capacitors, $E_{TCI}(C_A)$ and $E_{TCI}(C_B)$, and the energy dissipated in the resistor due to R_x being connected directly to ground, $E_{TCI}(R_x)$ during charging process. The upper limit of $E_{TCI}(R_x)$ would be given by:

$$E_{TCI}(R_x) = \frac{V_{Ach}^2}{R_x} T_{ch} \approx \frac{V_{DD}^2}{R_x} T_{ch} \tag{15}$$

The maximum total energy dissipated by the TCI in the estimation of R_x without considering the energy consumption of the DP, E_{TCI}, would therefore have an upper limit given by:

$$E_{TCI} = E_{TCI}(R_x) + E_{TCI}(C_A) + E_{TCI}(C_B) = \frac{V_{DD}^2}{R_x} T_{ch} + \frac{1}{2} C_A \left(\frac{C_B}{C_A + C_B} V_{DD}\right)^2 + \frac{1}{2} C_B \left(\frac{C_A}{C_A + C_B} V_{DD}\right)^2 = = \frac{V_{DD}^2}{R_x} T_{ch} + \frac{1}{2} C_{eq} V_{DD}^2 \tag{16}$$

Even taking $C_{eq} = C$, it is difficult to compare (4) and (16) as this depends on R_x and T_{ch}. However, it is clear that if T_{ch} is small enough, then $E_{TCI} < E_{TPCM}$. It is important to remember that T_{ch} in the TCI may be considerably lower than that used in other DICs in the literature, as these circuits require T_{ch} to be as long as necessary in order to equalize the initial voltages of all the discharging processes.

In any case, TCI acquisition time, $T_{M,TCI}$, is given by:

$$T_{M,TCI} = T_0 + T_{ch} + T_{A,\max} \tag{17}$$

where $T_{A,\max}$ is the value of T_A for the maximum R_x. Here, although T_0 may take values similar to T_{ch} to ensure complete discharge of the capacitors, it is evident that $T_{M,TCI} < T_{M,TPCM}$.

The requirements for the DP to be selected are minimal, with the only critical consideration being that it is able to establish values V_{Ach}, $V_{Bch} > V_{TL}$ when charging. Naturally, this will depend on the current that can be supplied by its pins, and on the resistance values to be measured not being too small. However, as will be shown in Section 4, it is not difficult to find DPs that can estimate resistance values of 200 Ω. These requirements must also be met by the DPs used in the second DIC proposal described below.

2.3. The Single-Capacitor Interface, SCI

The circuit is shown in Fig. 3 (a). As in the TCI, only two DP pins are used to control the process to estimate R_x. The circuit has a single capacitor, C, but two more resistors, R_A and R_B. Fig. 3 (b) shows the waveforms of V_A and V_B during the single charging-discharging process carried out by the circuit to estimate R_x. The first step, labeled number 1 in Fig. 3 (b), consists of charging C, selecting logic 1 in pin P_A, and setting pin P_B in Hi-Z state. Once again, the maximum voltage reached in the capacitor, $V_A = V_{Ach}$, is slightly lower than V_{DD} when charging, but in this case due to the ground connections of R_x and the equivalent resistance $R_A + R_B$. The final voltage stored in V_B, V_{Bch}, is given by

$$V_{Bch} = \frac{R_B \cdot V_{Ach}}{R_A + R_B} \tag{18}$$

It must be fulfilled that $V_{Bch} > V_{TL}$ as in the TCI, and the design condition is now:

$$\frac{R_A}{R_B} < \frac{V_{Ach}}{V_{TL}} - 1 \tag{19}$$

The same considerations regarding C_A and C_B with respect to (6) are valid for R_A and R_B with respect to (19). In terms of hardware, the capacitive voltage divider of the TCI is replaced by a resistive voltage divider in the SCI. However, it is important to note that the initial value of V_A in the charging process is not essential for the correct operation of the circuit, unlike in the TCI where it is necessary for V_A and V_B to be 0. This means it is not needed to use time T_0 to completely discharge C, as is the case in the TCI.

The second step in the estimation of R_x, labeled with number 2 in Fig. 3 (b), involves setting both pins in Hi-Z state in order to discharge C. Times T_A and T_B measured in this step again correspond to the intervals from the start of the discharge at the instants when $V_A = V_{TL}$ and $V_B = V_{TL}$ respectively. We can therefore write,

$$T_A = R_{eq} C \ln\left(\frac{V_{Ach}}{V_{TL}}\right) \tag{20}$$

$$T_B = R_{eq} C \ln\left(\frac{V_{Bch}}{V_{TL}}\right) = R_{eq} C \ln\left(\frac{R_B}{R_A + R_B} \cdot \frac{V_{Ach}}{V_{TL}}\right) \tag{21}$$

where $R_{eq} = R_x \,||\, (R_A + R_B)$. From (20) and (21) we can find the value of R_{eq}

$$R_{eq} = \frac{\Delta T}{C \ln\left(\frac{R_A + R_B}{R_B}\right)} \tag{22}$$

and finally

$$R_x = \frac{\lambda \cdot \Delta T}{\mu - \Delta T} \tag{23}$$

where λ and μ are known values that can be stored in the DP:

$$\lambda = R_A + R_B \tag{24}$$

$$\mu = (R_A + R_B) C \ln\left(\frac{R_A + R_B}{R_B}\right) \tag{25}$$

2.4. SCI analysis

The arithmetic complexity of (23) is similar to that of other DICs in the literature, but using only two measurements. Moreover, as shown in Fig. 3 (b), pin P_B is a simple DP input pin (it does not need to be configurable). This simplifies process control and frees up the DP's configurable pins. Moreover, the equivalent output resistor *ro* does not appear in any step in deducing (23).

As with (11), resolution in the estimation of R_x increases as resolution of $\triangle T$ increases. It can be seen in (20) and (21) that this is achieved by increasing R_{eq} and $(R_A + R_B)/R_B$, or equivalently by increasing $R_A + R_B$ and R_A/R_B with the limit set by (19).

Moreover, since (22) has the same form as (9), it is easy to obtain:

$$\frac{u(R_{eq})}{R_{eq}} \approx \frac{\sqrt{\alpha_A^2 + \alpha_B^2}}{V_{TL} \cdot \ln\left(\frac{R_A + R_B}{R_B}\right)} \tag{26}$$

Additionally,

$$u(R_{eq}) = \left|\frac{\partial R_{eq}}{\partial R_x}\right| u(R_x) = \left(\frac{R_{eq}}{R_x}\right)^2 u(R_x) \tag{27}$$

hence:

$$\frac{u(R_x)}{R_x} = \left(1 + \frac{R_x}{R_A + R_B}\right) \frac{u(R_{eq})}{R_{eq}} = \left(1 + \frac{R_x}{R_A + R_B}\right) \frac{\sqrt{\alpha_A^2 + \alpha_B^2}}{V_{TL} \cdot \ln\left(\frac{R_A + R_B}{R_B}\right)} \tag{28}$$

Since C does not appear in (28), as was the case in the TCI with C_{eq}, it does not make sense to increase C above a certain value in order to improve the quality of the estimates. The equation (28) also shows that, unlike the TCI, where $u(R_x)/R_x$ is independent of R_x, this parameter grows with R_x in the SCI, and is always larger than in the TCI (under the same operating conditions). However, if $R_x \ll R_A + R_B$, relative uncertainty is similar in both methods.

There are also two components in energy consumption: the energy dissipated in charging the capacitor, $E_{SCI}(C)$, and the energy dissipated in R_{eq}, $E_{SCI}(R_{eq})$. With the same considerations as for the TCI, the maximum limit for the energy dissipated by the SCI in an estimation of R_x without considering the energy consumption of the DP, E_{SCI}, is:

$$E_{SCI} = E_{SCI}(R_{eq}) + E_{SCI}(C) = \frac{V_{DD}^2}{R_{eq}} T_{ch} + \frac{1}{2} C V_{DD}^2 \tag{29}$$

In this equation, it has been considered that the initial voltage at the start of the charging process in C is 0. However, as shown in Fig. 3 (b), this is not really necessary since the charging process can start immediately after the instant trigger in node A, thus decreasing E_{SCI}.

As for SCI acquisition time, $T_{M,SCI}$, we have:

$$T_{M,SCI} = T_{ch} + T_{A,\max} \tag{30}$$

Since T_0 does not appear in the expression, it is obvious that the estimations are faster in the SCI than in the TCI for $C_{eq} \approx C$.

Finally, C_A, C_B, R_A, R_B, and C change with temperature, and these variations affect the estimates (9) and (23). However, by choosing elements with the same characteristics, the terms that are ratios of resistors and capacitors in (9) and (23) are not affected by these variations. Since C_{eq} varies in the same way as C_A or C_B, the relative variations in the estimate of R_x with temperature in the TCI are identical to those of the capacitors used (about 30 ppm/K for NPO capacitors). However, in the SCI, both the resistors and the capacitor contribute to the error in the estimate due to temperature variations.

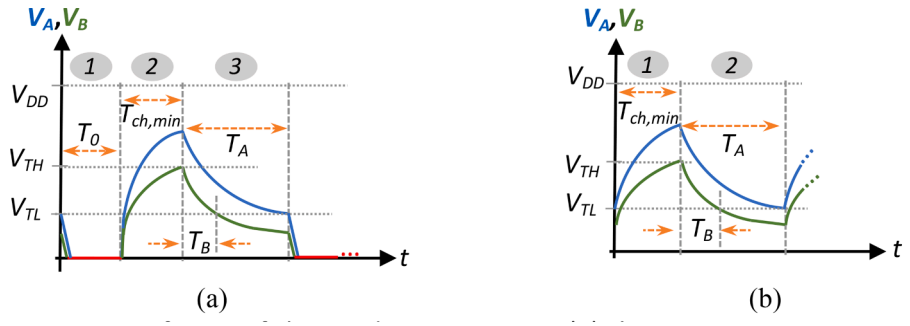

Fig. 4. Waveforms of the readout process in (a) the Two-Capacitor Interface circuit with unfixed charging time (TCI-U) and (b) the Single-Capacitor Interface circuit with unfixed charging time (SCI-U).

2.5. Reducing measurement acquisition time

When required, further increases in data acquisition frequency can be achieved by reducing T_{ch}. The TCI or the SCI actually only needs sufficient T_{ch} for $V_B > V_{TL}$. Finding the instant when this happens during charging is not possible, although we can identify the instant when $V_B > V_{TH}$, $T_{ch,\min}$, where V_{TH} is the threshold voltage to detect a logic 1 in the P_B pins of Figs. 2 (a) and 3 (a) ($V_{TH} > V_{TL}$). As $V_A > V_B$ in the charging process, charging can be terminated after a time $T_{ch,\min}$ and a discharging process performed to obtain T_A and T_B. To differentiate, DICs with a fixed charging time will be referred to as TCI-F and SCI-F, as shown in Fig. 2(b) and 3(b), while TCI-U and SCI-U will be used to refer to DICs with unfixed charging times where the length of charging time is chosen automatically, as described above. The evolution over time of the charging process for the TCI-U is shown in Fig. 4 (a), and for the SCI-U in Fig. 4 (b). In any case, the equations to estimate R_x are still (11) and (23).

As shown in Fig. 4, V_{Ach} can be significantly lower than V_{DD}. Hence, if no other circuit parameter is modified, power consumption for the same value of R_x decreases in the TCI-U and in the SCI-U with respect to the TCI-F and the SCI-F. This is also the reason why T_A and T_B are lower in the TCI-U and in the SCI-U. As a result, the importance of quantization error in these versions may increase and resolution may worsen. This is the price to pay for an increase in measurement acquisition speed.

3. Materials and methods

We have chosen an FPGA, the Xilinx Artix 7 XC7A35T, as the DP to test the new resistive DIC, meaning we have included the new DICs within devices with high computing capacity. This method allows the estimations made by the TCI or the SCI to be used in high-level applications implemented within the same FPGA, giving rise to a real smart sensor. The FPGA is part of the CMOD A7 board from Digilent (Pullman, Washington), together with a USB-UART bridge, a clock source, 512 KB SRAM, 4 MB Quad SPI Flash, and several I/O devices. The supply voltage is $V_{DD} = 3.3$ V, and the frequency clock used internally in the FPGA is 50 MHz. Thanks to the versatility of the FPGA, the implemented design uses both the rise and fall edges of the clock to detect the trigger instant.

Twenty-six high-precision resistors from 221.06 Ω to 24.878 kΩ were used for the measurements of R_x. This wide range of values (41 dB) includes the operating ranges of a large number of resistive sensors. For the TCI, $C_A = 90.25$ nF and $C_B = 99.73$ nF have been selected to meet the design constraint (6). For the SCI, we have chosen $R_A = 15{,}014$ Ω and $R_B = 12{,}701$ Ω to meet the design constraint (19) and to ensure that $R_A + R_B > R_x$ reducing $u(R_x)/R_x$, as shown in (28). All resistors and capacitors were measured with a digital LCR meter (LCR-6002 from RS PRO). It is important to note that V_{Ach}/V_{TL} is not a known value since it slightly depends on R_x. However, since V_{Ach} is close to V_{DD} and the experimentally determined value of V_{TL} is 1.26 V, then the term $V_{Ach}/V_{TL} - 1$ that appears in (6) and (19) is a lower value but close to 1.62. In any case, the choices $C_B/C_A = 1.11$ and $R_A/R_B = 0.85$ are very conservative, with values far from this limit. Moreover, $C_{eq} = 47.38$ nF has been selected in the TCI and C = 46.65 nF in the SCI (commercial capacitors could not be found in order to further equalize the values in both circuits). With these choices, T_A and T_B are quite similar in the same versions of the TCI and the SCI for the same R_x.

In the case of the TCI-F and the SCI-F, $T_{ch} = 40$ μs has been chosen to stabilize the value of V_{Ach} around the maximum possible. It has also been selected $T_0 = 40$ μs in both versions of the TCI. This time coincides, approximately, with the values of T_A if R_x is about 1 kΩ. The maximum value of T_A for the selected resistance range is about 1.12 ms. For the TCI-U and the SCI-U, $T_{ch,\min}$ differs slightly in both versions but is between 2.5 μs and 4.5 μs.

Finally, 20 series of 500 estimates were made for each resistor, with approximately 2 s between each series.

4. Experimental results and discussion

The results in this section have been obtained considering the series with the highest relative error, e_R, from the 500 estimations in this series. The figure of merit, e_R, for the estimation of R_x is defined by

$$e_R = \mathrm{Max}\left(\frac{|R_x(i) - R_{x,a}|}{R_{x,a}} \times 100\%\right); \quad i \in \{1, \ldots, 500\} \tag{31}$$

where $R_x(i)$ is each of the estimations of R_x, whether using (11) or (23). $R_{x,a}$ is the actual resistance value measured by the LCR meter. The results for e_R in the case of the TCI-F and the SCI-F are shown in Fig. 5 (given the wide range of R_x, this and the following figures are shown on the X-axis in a log scale). The figure also shows systematic error, e_S, defined as

$$e_S = \frac{|\overline{R} - R_{x,a}|}{R_{x,a}} \times 100\% \tag{32}$$

where $\overline{R}$ is the average of the 500 $R_x(i)$.

The first note of interest is that e_R is higher in the SCI-F than in the TCI-F for almost all R_x values. The difference is most evident outside the R_x intermediate values zone. The low values zone of R_x presents the highest e_R in both methods and the greatest difference between them. This is due to the increasing importance of quantization errors as T_A and T_B decrease. These times are shorter in the SCI-F, meaning errors are larger in this DIC. In any case, the maximum e_R for the TCI-F is 0.4 %, and 0.78 % for the SCI-F. Fig. 5 also shows e_S for both methods; e_S moves within a small range in both methods, except in the region where quantization errors are important.

As shown in Fig. 6, relative and systematic errors in the TCI-U and the SCI-U are very similar to those in Fig. 5. Since V_{Ach} is lower, the measured times are shorter in the TCI-U and the SCI-U. Thus, due to quantization errors, e_R and e_S are more significant in the lower part of the range in Fig. 6 than in Fig. 5 (now maximum e_R is 1.7 %). However, as expected, the errors are almost identical in both figures in the upper

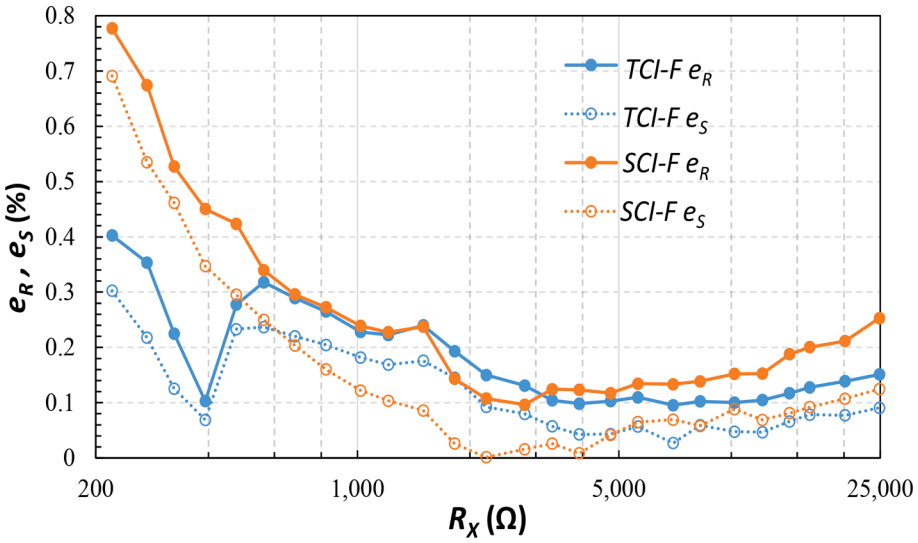

Fig. 5. Relative and systematic errors, e_R and e_S, for the new proposed DICs, TCI-F and SCI-F. The X-axis, in log5 scale, shows the resistances under test.

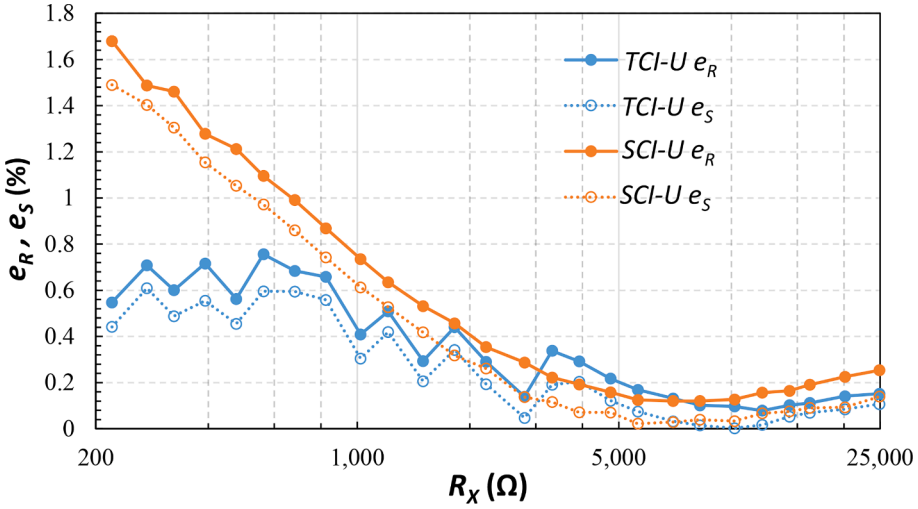

Fig. 6. Relative and systematic errors, e_R and e_S, for the fastest versions of DICs, TCI-U and SCI-U.

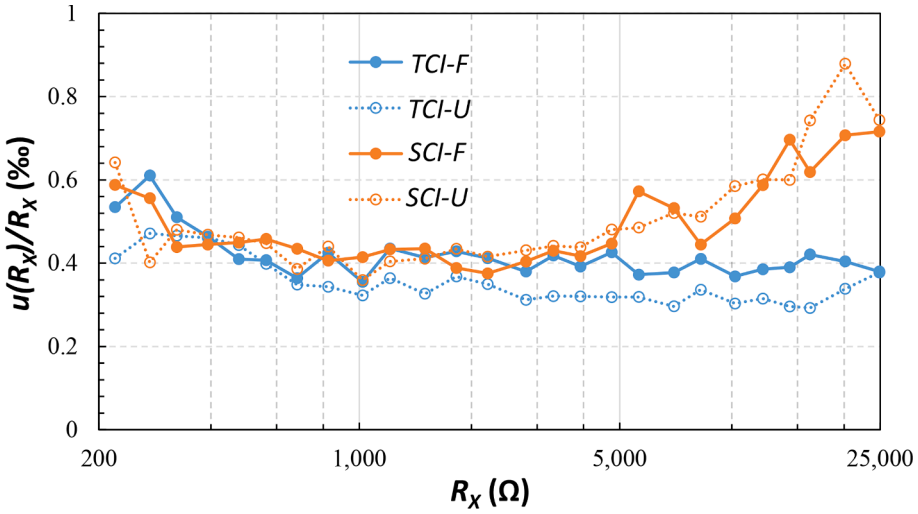

Fig. 7. Relative uncertainty in the estimate of R_x expressed in ‰. As of 5 kΩ this figure of merit is higher for the SCI versions.

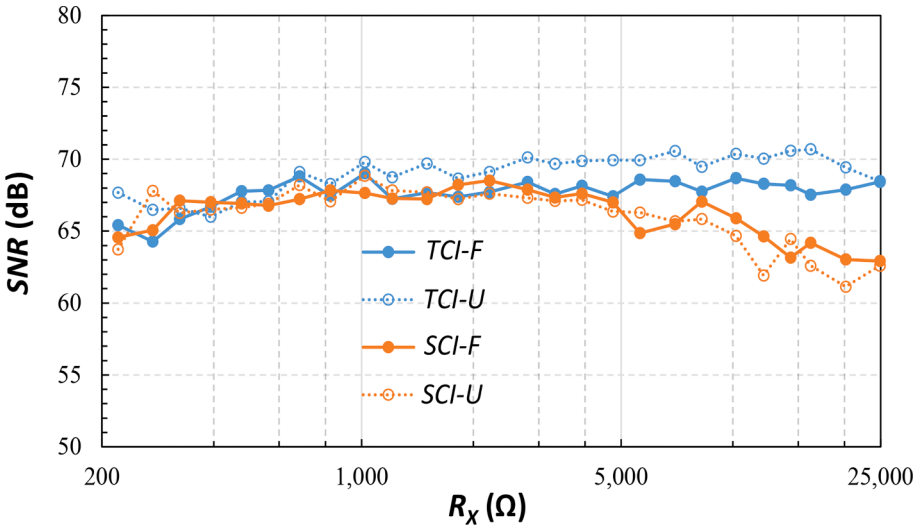

Fig. 8. Signal-to-noise ratio, SNR, of the circuit showing very stable values for the TCI proposals. In the case of SCI proposals, SNR worsens slightly for highest resistance values.

Table 1
Maximum Acquisition Time, T_M, in the new DICs.

Type	T_0	T_{ch}	T_A	T_M
TCI-F	40 µs	40 µs	1126 µs	1206 µs
TCI-U	40 µs	4 µs	966 µs	1010 µs
SCI-F	–	40 µs	645 µs	685 µs
SCI-U	–	3 µs	589 µs	592 µs

Table 2
Energy Consumption in the new DICs.

Type	*Average Energy Consumption by R_x estimation*
TCI-F	476 nJ
TCI-U	180 nJ
SCI-F	494 nJ
SCI-U	187 nJ

part of the R_x range. In other words, increasing data acquisition frequency using the TCI-U and the SCI-U comes at the cost of an increase in errors for low resistance values.

It is also interesting to note that the difference between e_R and e_S for high values of R_x is greater in the SCI than in the TCI in both Fig. 5 and Fig. 6. This coincides with the result of (28), which predicts an increase of $u(R_x)/R_x$ with the value of R_x.

Fig. 7 shows $u(R_x)/R_x$ in the four proposed DIC versions. Relative uncertainty is approximately constant over the entire range of R_x for the TCI, as predicted by (14), while for the SCI the increase discussed above is observed for the higher values of R_x. The figure shows how a clear difference between the uncertainties of the TCI and those of the SCI can be seen from 5 kΩ onwards. Although the TCI is slower, requiring time T_0 to fully discharge the capacitors, it nevertheless produces better estimations for high resistance values than the SCI. In other words, there is a trade-off between acquisition speed and accuracy/precision. Hence, the fastest version of the new DICs, SCI-U, is also the one with the highest errors.

Fig. 8 shows the results for the signal-to-noise ratio (SNR) of the new DICs, calculated as:

$$SNR = 10\cdot\log\left(\frac{\sum_i R_x(i)^2}{\sum_i [R_x(i)-\overline{R}]^2}\right); \quad i \in \{1,\ \ldots,\ 500\} \tag{33}$$

As expected from the results presented in the figures above, SNR is also very stable over the entire range of R_x for the TCI proposals. At the same time, SNR worsens slightly for higher resistance values in the SCI proposals. Whatever the DIC analyzed, SNR is consistently above 60 dB in the SCI and 64 dB in the TCI.

As for T_M, Table 1 shows its values for the different proposals. The times were obtained by performing isolated measurements in which the capacitors are discharged completely at the end of the measurement process.

Logically, for the same circuit, T_M is higher in DICs with fixed T_{ch}. In the case of the TPCM, assuming T_{ch} = 40 µs, C = 47 nF, and the completion of an isolated measurement, this has been obtained theoretically using (3) $T_{M,TPCM}$ = 2372 µs. In other words, the slowest version of the new DICs, the TCI-F, reduces the maximum estimation time of the TPCM by almost half, while the fastest version, SCI-U, reduces it by 75

Table 3
Comparison between the TPCM in [22] and the new DICs.

	TPCM	TCI-F	SCI-F	TCI-U	SCI-U
Passive Components	2-R, 1-C	2-C	2-R, 1-C	2-C	2-R, 1-C
Used Pins of DP	3	2	2	2	2
Range of R_x	800 Ω - 1500 Ω	221 Ω – 24.9 kΩ	221 Ω – 24.9 kΩ	221 Ω – 24.9 kΩ	221 Ω – 24.9 kΩ
Charging + Discharging Cycles	6	3	2	3	2
Measurements Required	3	2	2	2	2
e_S (%) for R_x in 221 Ω – 24.9 k Ω range	–	0.3 %	0.7 %	0.6 %	1.5 %
e_S (%) for R_x in 800 Ω – 1500 Ω range	0.22 %	0.2 %	0.16 %	0.58 %	0.75 %
Maximum Acquisition Time, T_M	2372 µs	1206 µs	685 µs	1010 µs	592 µs
Energy Consumption	768 nJ	476 nJ	494 nJ	180 nJ	187 nJ

%.

Meanwhile, energy consumption depends on R_x in all versions. For example, Table 2 shows the theoretical average energy consumption in estimating all resistance values in the range for each new proposal according to (4), (16) and (29). The results in Table 2 can be compared with the energy consumed in the three charging processes carried out for a 47 nF capacitor in the TPCM, where the energy consumed is independent of R_x, totaling 768 nJ. The smallest reduction is for the SCI-F, 35 %, while the largest is for the TCI-U, 76 %. The results in Table 2 show a large difference in energy consumption between the versions with fixed T_{ch} and the others. In any case, the differences shown in Table 2 are insignificant compared to the energy consumption of the latest generation FPGAs. However, these differences become relevant if an ultra-low-power microcontroller is used as DP. The designer should assess these consumption levels, together with the accuracy shown in Figs. 5 and 6 and the value of T_M in Table 1, in order to decide which version to use in a given application. In any case, the four versions provide a range of options for the designer.

Table 3summarizes, for comparison purposes, the main figures of merit of the TPCM in [22] and the proposed new DICs. Because the R_x ranges are different, the maximum systematic errors for the range of each DIC and for the range common to all of them are shown in two different rows. T_M and Energy Consumption are estimated for the TPCM in the 221 Ω – 24.9 kΩ range.

5. Conclusions

Direct Interface Circuits (DICs) are efficient circuits to digitize the resistance value of a resistive sensor, R_x. Some of them use only passive components and a digital processor, DP, to estimate R_x. These circuits actually perform a resistance-to-time-to-digital conversion. Several calibration resistors and several charging-discharging cycles of a capacitor are required to perform this conversion. The most accurate DIC versions require three calibration resistors, three charging-discharging cycles, and three to six time measurements to obtain an estimate.

This paper represents two new DICs, the Two-Capacitor Interface (TCI) and the Single-Capacitor Interface (SCI), which perform the resistance-to-time-to-digital conversion more efficiently since:

1) They can require fewer components: the SCI uses, in addition to the DP, the same number of elements as previous versions of DICs, two resistors and a capacitor of known value. The TCI, however, only needs two capacitors of known value.
2) Only two DP pins are required to perform the resistance reading, as opposed to, for example, the four used in the Two-Point Calibration Method.
3) The TCI and the SCI only require one charging and discharging cycle to estimate R_x. In the case of the TCI, the two capacitors have to be discharged completely, while for the SCI it is not necessary to completely discharge the circuit's only capacitor.
4) The TCI and the SCI only use two time measurements, both performed during the single discharge, to estimate R_x, thus reducing the possible sources of error (including the output resistance of the DP pins *ro*, or the need to equalize capacitor voltages at the start of the discharging processes). Furthermore, the TCI has the simplest R_x estimation equation among those proposed in the literature, which decreases the DP's workload.
5) Estimation is faster, and the energy consumption is lower since only a single charging-discharging process is required.

Funding

This work was supported by the Spanish Government under contract PID2021-125091OB-I00. Funding for open access charge: Universidad de Málaga / CBUA.

CRediT authorship contribution statement

José A. Hidalgo-López: Conceptualization, Methodology, Validation, Investigation, Writing - review & editing. **Julián Castellanos-Ramos:** Methodology, Software, Validation, Investigation, Writing - review & editing.

Declaration of Competing Interest

The authors declare that they have no known competing financial interests or personal relationships that could have appeared to influence the work reported in this paper.

Data availability

Data will be made available on request.

References

[1] Y. Moser, M.A.M. Gijs, Miniaturized flexible temperature sensor, J. Microelectromechanical Syst. 16 (6) (Dec. 2007) 1349–1354.
[2] J. Marek Smulko, et al., New approaches for improving selectivity and sensitivity of resistive gas sensors: a review, Sens. Rev. 35 (2015) 340–347.
[3] R. Pierce and G. Sen Gupta, "Investigation of force sensors for use in bipedal humanoid dynamic gait generation," *2014 IEEE Sensors Appl. Symp. SAS 2014 - Proc.*, pp. 289–292, 2014.
[4] D. Sherman, Measure Resistance and Capacitance without an A/D, AN449, Sunnyvale, CA, 1993.
[5] A. Webjörn, "Simple A/D for MCUs without built-in A/D converters, AN477," Milton Keynes, UK, 1993.
[6] K. Elangovan, A.C. Sreekantan, Evaluation of new digital signal conditioning techniques for resistive sensors in some practically relevant scenarios, IEEE Trans. Instrum. Meas. 70 (2021) 1–9.
[7] Z. Kokolanski, C. Gavrovski, V. Dimcev, Modified single point calibration with improved accuracy in direct sensor-to-microcontroller interface, Meas. J. Int. Meas. Confed. 53 (2014) 22–29.
[8] O. Lopez-Lapeña, E. Serrano-Finetti, O. Casas, Low-power direct resistive sensor-to-microcontroller interfaces, IEEE Trans. Instrum. Meas. 65 (1) (2016) 222–230.
[9] L. Bengtsson, Direct analog-to-microcontroller interfacing, Sensors Actuators, A Phys. 179 (2012) 105–113.
[10] A. Depari, et al., Minimal Wide-Range Resistive Sensor-to-Microcontroller Interface for Versatile IoT Nodes, IEEE Trans. Instrum. Meas. 71 (2022).
[11] Z. Kokolanski, C. Gavrovski, V. Dimcev, M. Makraduli, Hardware techniques for improving the calibration performance of direct resistive sensor-to-microcontroller interface, Metrol. Meas. Syst. 20 (4) (Dec. 2013) 529–542.
[12] F. Reverter, "Interfacing sensors to microcontrollers: a direct approach", in *Smart Sensors and MEMs*, Woodhead Publishing, Second., 2018, pp. 23–55.
[13] A. Custodio, R. Pallas-Areny, R. Bragos, Error analysis and reduction for a simple sensor-microcontroller interface, IEEE Trans. Instrum. Meas. 50 (6) (2001) 1644–1647.
[14] P.R. Nagarajan, B. George, V.J. Kumar, Improved single-element resistive sensor-to-microcontroller interface, IEEE Trans. Instrum. Meas. 66 (10) (Oct. 2017) 2736–2744.
[15] A. Anarghya, S.S. Rao, M.A. Herbert, P. Navin Karanth, N. Rao, Investigation of errors in microcontroller interface circuit for mutual inductance sensor, Eng. Sci. Technol. an Int. J., Apr. 22 (2) (2019) 578–591.
[16] Ó. Oballe-Peinado, J. A. Hidalgo-López, J. A. Sánchez-Durán, J. Castellanos-Ramos, and F. Vidal-Verdú, "Architecture of a tactile sensor suite for artificial hands based on FPGAs," in *Proceedings of the IEEE RAS and EMBS International Conference on Biomedical Robotics and Biomechatronics*, 2012.
[17] J.A. Hidalgo-López, J.A. Botín-Córdoba, J.A. Sánchez-Durán, Ó. Oballe-Peinado, Fast Calibration Methods for Resistive Sensor Readout Based on Direct Interface Circuits, Sensors 19 (18) (2019) 3871.
[18] Z. Kokolanski, F. Reverter Cubarsí, C. Gavrovski, V. Dimcev, Improving the resolution in direct inductive sensor-to-microcontroller interface, Annu. J. Electron. 9 (2015) 135–138.
[19] Z. Kokolanski, M. Gasulla, and F. Reverter, "Differential Inductive Sensor-to-Microcontroller Interface Circuit," in *2019 IEEE International Instrumentation and Measurement Technology Conference (I2MTC)*, pp. 1–5.
[20] Z. Czaja, Time-domain measurement methods for R, L and C sensors based on a versatile direct sensor-to-microcontroller interface circuit, Sensors Actuators A Phys. 274 (May 2018) 199–210.
[21] Z. Czaja, Measurement method for capacitive sensors for microcontrollers based on a phase shifter, Meas. J. Int. Meas. Confed. vol. 192 (2022), 110890.
[22] F. Reverter, J. Jordana, M. Gasulla, R. Pallàs-Areny, Accuracy and resolution of direct resistive sensor-to-microcontroller interfaces, Sensors Actuators, A Phys. 121 (1) (May 2005) 78–87.
[23] F. Reverter, M. Gasulla, R. Pallas-Areny, R. Pallàs-Areny, Analysis of power-supply interference effects on direct sensor-to-microcontroller interfaces, IEEE Trans. Instrum. Meas. 56 (1) (2007) 171–177.

[24] J.A. Hidalgo-Lopez, J.A. Botin-Cordoba, J.A. Sanchez-Duran, J.C. Tejero-Calado, O. Oballe-Peinado, Improved Calibration Method for Resistive Sensors using Direct Interface Circuits, IEEE Trans. Instrum. Meas. 69 (8) (2020) 5693–5701.
[25] F. Reverter, R. Pallàs-Areny, Uncertainty reduction techniques in microcontroller-based time measurements, Sensors Actuators A Phys. 127 (1) (2006) 74–79.
[26] J.A. Hidalgo-Lopez, J.A. Sanchez-Duran, O. Oballe-Peinado, Method to Reduce Quantization Error in Direct Interface Circuits for Resistive Sensors, IEEE Sens. J. XX (XX) (2020) 1.
[27] J.A. Hidalgo-López, Ó. Oballe-Peinado, J. Castellanos-Ramos, J.A. Sánchez-Durán, Two-capacitor direct interface circuit for resistive sensor measurements, Sensors 21 (4) (Feb. 2021) 1–17.